

Wavefront correction based on a reflective liquid crystal wavefront sensor

This article has been downloaded from IOPscience. Please scroll down to see the full text article.

2009 J. Opt. A: Pure Appl. Opt. 11 015511

(<http://iopscience.iop.org/1464-4258/11/1/015511>)

View the [table of contents for this issue](#), or go to the [journal homepage](#) for more

Download details:

IP Address: 159.226.165.151

The article was downloaded on 05/09/2012 at 10:15

Please note that [terms and conditions apply](#).

Wavefront correction based on a reflective liquid crystal wavefront sensor

L Hu¹, L Xuan, D Li, Z Cao, Q Mu, Y Liu, Z Peng and X Lu

State Key Laboratory of Applied Optics, Changchun Institute of Optics, Fine Mechanics and Physics, Dong Nanhu street, 16, Changchun, Jilin 130033, People's Republic of China

E-mail: hulifa@ciomp.ac.cn

Received 9 August 2008, accepted for publication 8 December 2008

Published 30 December 2008

Online at stacks.iop.org/JOptA/11/015511

Abstract

A novel wavefront sensor (WFS) based on liquid crystal on silicon (LCOS) is demonstrated. The design of the liquid crystal microlens array with LCOS is given in detail. To save the energy of the incident light, an optimized optical design of the WFS is also considered. In addition, closed loop wavefront correction experiments were conducted based on the designed LC WFS with square and hexagonal microlens arrays, respectively. In the experiment, the corrector was a tilt and tip mirror. The results indicated that the Zernike coefficients of the tilt and tip were decreased to less than 0.1λ (633 nm) after correction.

Keywords: wavefront sensor, adaptive optics, liquid crystals

1. Introduction

Shack–Hartmann wavefront sensors (SH WFSs) have been used for many applications, such as adaptive optics in astronomy, ophthalmic metrology, laser beam characterization, optical system alignment, an optical metrology for both large and small optics [1–4]. An SH WFS consists of a microlens array and a charge-coupled device (CCD). The wavefront can be accurately calculated from the slopes of every subaperture [5–8].

Unlike a conventional microlens, the liquid crystal (LC) microlens produced by LC space light modulators are programmable, as demonstrated by some researchers [9–13]. Although there have been experimental or theoretical investigations of wavefront sensors based on transmissive LC devices, there are several problems. First, the LC microlens array is based on a twisted nematic (TN) LC. Unfortunately, a TN LC will lead to a complex optical layout and a high energy loss. In fact, a TN LC generally operating in a phase mostly mode has some amplitude modulation on the incident light. In addition, for TN LC devices, part of the incident light could not be modulated by the LC without a gray grating as a background to filter the non-modulated light in the zeroth order. Therefore, the centroid calculation precision of the local light spot based on such a kind of LC microlens will decrease. Second, available transmissive LC devices have large pixel size

and low filling factor, which will lead to low energy efficiency. To avoid these problems, in this paper, we demonstrate the LC WFS based on a reflective phase-only LC space light modulator with parallel alignment LC. We also present a new optical design to decrease the incident light loss for LC WFSs.

In this paper, we design a reflective LC WFS based on LCOS, and use it to control a tilt and tip mirror to correct an aberrated wavefront in a laboratory. First, we discuss the design of the LC WFS and its wavefront reconstruction in section 2. Second, we present the tilt and tip correction method, and discuss the wavefront correction results based on the LC WFS in section 3. Finally, a conclusion is given in section 4.

2. Theory

2.1. LC microlens design

The design parameters of the LC WFS can be changed flexibly to satisfy a specific application. The focal length, position, size, arrangement, and number of LC microlenses can be changed by applied a specific gray map on the LCOS. To generate an array of LC microlens, the Fresnel lens function written onto each pixel of an LCOS is

$$z(x, y) = c \left(\left(\frac{x - x_i}{d} \right)^2 + \left(\frac{y - y_i}{d} \right)^2 \right) \quad (1)$$

¹ Author to whom any correspondence should be addressed.

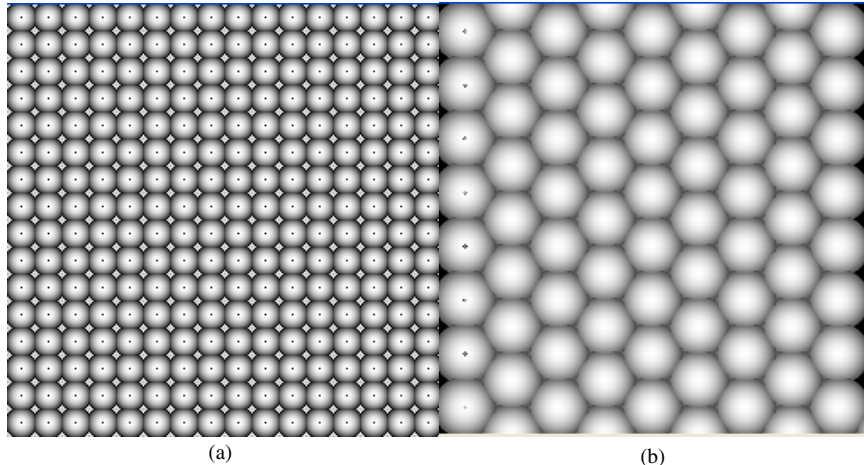


Figure 1. LC microlens demonstration: (a) square, (b) hexagonal.

where x and y are the coordinates along the X and Y axes in units of pixel, respectively; x_i and y_i are the center coordinates along the X and Y axes for the i th LC microlens, respectively; d is the radius of the LC microlens; and c is a constant that determines the peak vale (PV) value of the wavefront produced. In addition, because it is necessary for the LCOS to produce a wavefront with the binary optics method, the diffraction efficiency is very important. The relationship between the number of phase levels and the diffraction efficiency of the first order is as follows [14, 15]:

$$\eta_{\max}(m) = \left[\frac{m}{\pi} \sin\left(\frac{\pi}{m}\right) \right]^2 \quad (2)$$

where η_{\max} is the diffraction efficiency of the first order; m is the number of phase levels. Therefore, η_{\max} is 95% for $m = 8$, and 81% for $m = 4$. To produce a precise wavefront for the microlens array, the number of phase levels should be larger than 8.

Figure 1 shows the gray maps for two kinds of LC microlens. The LC microlens gray maps for square and hexagonal arrangements are shown in figures 1(a) and (b). It should be noted that every LC microlens is generated with the phase wrapping method, which leads to black spots in the center of the microlens. Their corresponding specific parameters are shown in table 1. Every microlens for the square arrangement LC WFS consists of 32 pixels \times 32 pixels, and the diameter of every microlens for the hexagonal arrangement LC WFS is 64 pixels. Theoretically, the diffractive efficiency is more than 99%. The pixel size of the CCD is 15 μm . Therefore, the real radius d of every microlens could be obtained by multiplying the pixel size by the pixel number of the subarea. Table 1 shows the specific parameters of the LC microlens with square and hexagonal arrangements, where d is the radius of the LC microlens, and h is the theoretical wavefront PV value of a single LC microlens. The effective focus lengths are long. Therefore, the space occupied by the whole wavefront sensor is absolutely larger than that of available conventional WFS configurations, which is the main drawback of the reflective LC WFS. Meanwhile, the dynamic range of the presented wavefront sensor is also

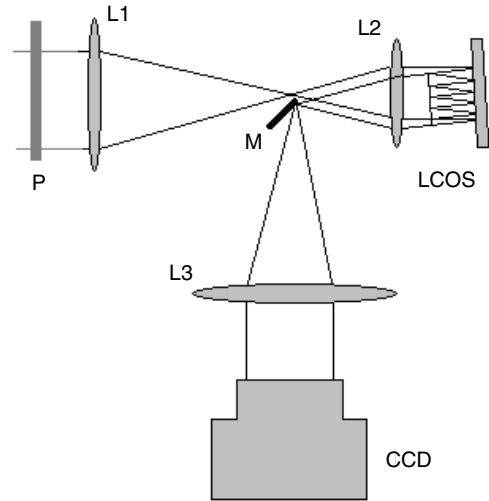


Figure 2. The LC wavefront sensor setup.

Table 1. Specification for different LC microlens arrangements.

LC microlens	Sub area (pixel)	d (mm)	h (633 nm)	Focus length (mm)
Square	32 \times 32	0.240	0.7	65
Hexagonal	64	0.480	0.9	202

estimated to be very small with these long focal lengths. However, improvement in optical layout optimization design and LC microlens design will lead to an increase in its dynamic range, that is, use a direction dependent grating as a gray map on LCOS to enlarge the sub area of every microlens on CCD.

2.2. Wavefront reconstruction [16–19]

After the CCD detector grabs the spot image, the following steps are necessary to reconstruct the wavefront. First, we use the centroid computation approach to determine the center of the spot. The center positions C_x and C_y of the spot along the x and y directions can be calculated according to a traditional

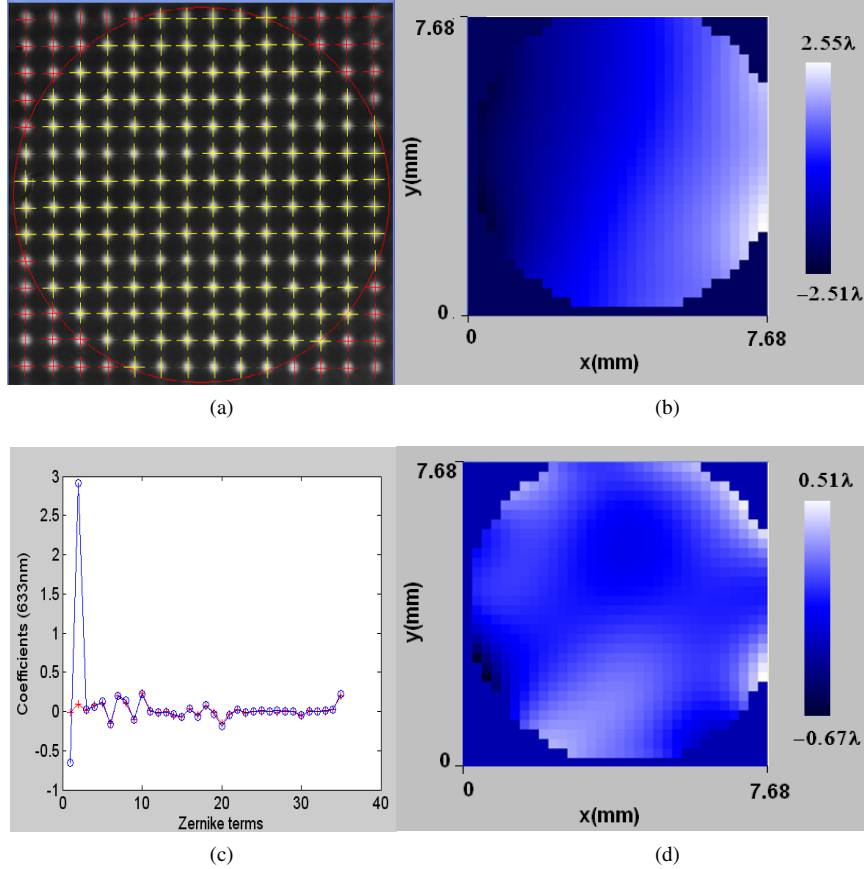


Figure 3. Measured wavefronts and light point array for a square LC microlens: (a) light point array with size $7.68 \times 7.68 \text{ mm}^2$, (b) wavefront before correction, $\text{PV} = 5.06\lambda$, $\text{rms} = 2.22\lambda$, (c) the first 35 Zernike coefficients before (blue circle) and after (red star) correction, (d) wavefront after correction, $\text{PV} = 1.17\lambda$, $\text{rms} = 0.25\lambda$.

gravity center algorithm. Therefore, the slopes along the X and Y axes corresponding to every microlens could be obtained as

$$S_x = \frac{C_{x,s} - C_{x,r}}{f} \quad (3)$$

$$S_y = \frac{C_{y,s} - C_{y,r}}{f} \quad (4)$$

where f is the focal length of the LC microlens. According to equations (3) and (4), from every frame of light points acquired by the CCD, we could obtain an array S of slopes corresponding to every microlens:

$$S = [s_{1,x}, \dots, s_{n,x}, \dots, s_{1,y}, \dots, s_{n,y}] \quad (5)$$

where n is the total number of the reference light points on the CCD. On the other hand, we have to calculate the response functions for every modal of the Zernike polynomial so as to reconstruct the wavefront. In this paper, we use the first 35 modals of the OSA Zernike polynomial. The response function could be calculated with the following equation:

$$R_{35 \times 2n} = \begin{bmatrix} \frac{\partial Z_{1,1}(x,y)}{\partial x}, \dots, \frac{\partial Z_{1,n}(x,y)}{\partial x}, \frac{\partial Z_{1,1}(x,y)}{\partial y}, \dots, \frac{\partial Z_{1,n}(x,y)}{\partial y} \\ \vdots \\ \frac{\partial Z_{35,1}(x,y)}{\partial x}, \dots, \frac{\partial Z_{35,n}(x,y)}{\partial x}, \frac{\partial Z_{35,1}(x,y)}{\partial y}, \dots, \frac{\partial Z_{35,n}(x,y)}{\partial y} \end{bmatrix}. \quad (6)$$

It should be noted that partial derivation relative to x and y for every subarea should be summed for every pixel position and averaged so as to improve the slope calculation precision. Then, from equation (6), the command matrix for wavefront reconstruction could be calculated as

$$M_{2n \times 35} = (R^T R)^{-1} R. \quad (7)$$

Therefore, from equations (5) and (7), the Zernike modal coefficients could be determined by

$$A = S_{1 \times 2n} \cdot M_{2n \times 35} \quad (8)$$

where A is an array of Zernike coefficients. According to A , it is very easy to calculate the wavefront as

$$Z = \sum_{i=1}^{35} a_i Z_i(x, y). \quad (9)$$

2.3. LC WFS system design

Compared with a traditional WFS [20], the LC WFS has two main differences: first, it is polarization dependent because of the LC material; next, the LCOS is reflective. If one uses a beam splitter between the LCOS and the CCD, the loss of incident light energy will not be avoided. Therefore, we designed an optical layout as shown in figure 2. It should be

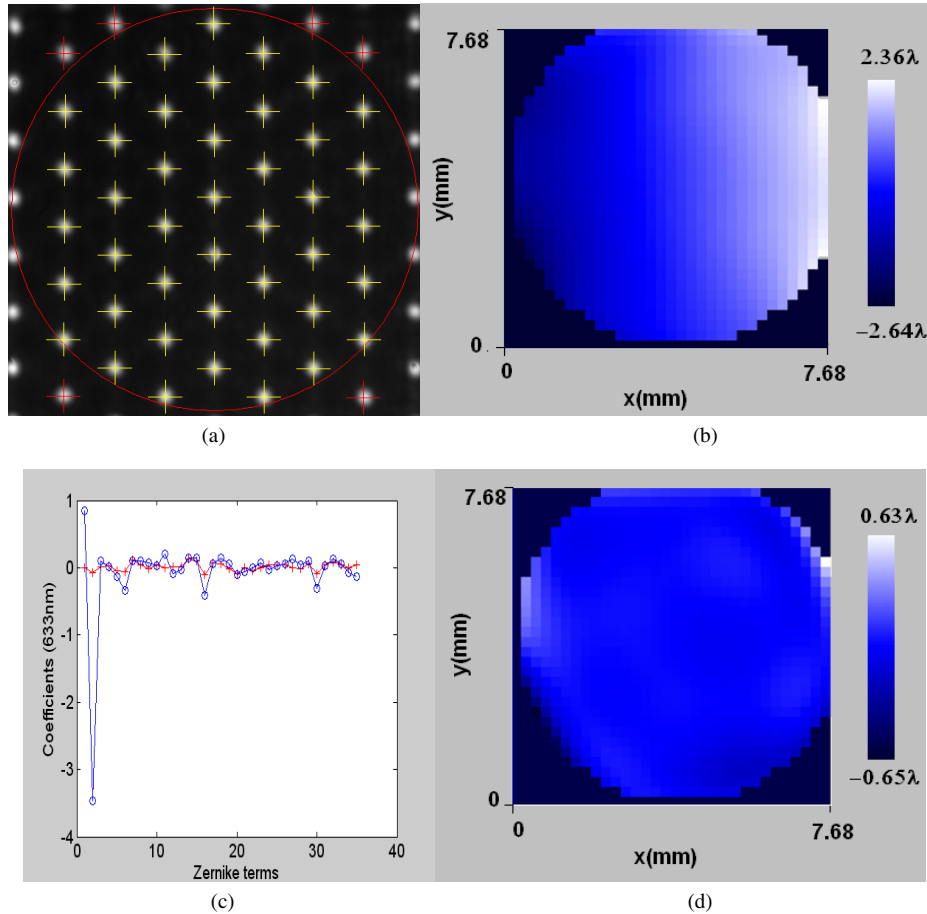


Figure 4. Measured wavefronts and light point array for a hexagonal LC microlens: (a) light point array with size $7.68 \times 7.68 \text{ mm}^2$, (b) wavefront before correction, $\text{PV} = 5.01\lambda$, $\text{rms} = 2.09\lambda$, (c) the first 35 Zernike coefficients before (blue circle) and after (red star) correction, (d) wavefront after correction, $\text{PV} = 1.28\lambda$, $\text{rms} = 0.20\lambda$.

noted that a polarization beam splitter (PBS) could be used to obtain linear polarization light if the incident light is non-polarized. But if the incident light is polarized, the PBS should be replaced just by a beam splitter (BS). One part of incident light is used for wavefront sensing; the other is for imaging. Lenses L1 and L2 could lead to a reasonable area on the LCOS for the incident light. In addition, the LCOS is not vertical to the incident light. The angle between the incident light and the plane of the LCOS is less than about 5° . Our previous experimental results indicated that the phase modulation characteristics of the LCOS will not change under such small angles. Then, the focus of the reflected light by the LCOS through lens L2 again will have a displacement. It is reflected by mirror M, and finally reaches the CCD1. This kind of design avoids energy loss as much as possible. The main energy loss of our LC WFS is due to the LCOS's relatively low reflectivity. Although the LC has dispersion in the visible band, its effects may be neglected for our LC lens with large focus ratio.

Another problem is that the reflective light from the edge of the LCOS possibly includes part of the light reflected by the glass. Therefore, a reasonable focus length of lens L3 should be chosen to let the light from the four edges of the LCOS be outside the detection range of the CCD. In our experiments,

the LCOS is from Boulder nonlinear systems. Its pixel size is $15 \times 15 \mu\text{m}^2$, and its format is 512×512 . The CCD is a DU897 from Andor Technology.

3. Experiments and discussion

To validate our design, a closed loop adaptive optical system including our LC WFS and a tilt and tip mirror was built. The aim is to measure the wavefront slopes with our LC WFS to correct the tilt and tip aberration in an optical layout with an S-330 mirror from PI Company during closed loop correction. It should be noted that the tilt and tip aberration is static and is generated manually by one reflective mirror in the system, not generated by the LCOS. Based on the above theory, we designed two kinds of LC WFS with different LC microlens array arrangements, as shown in figure 1: one has a square microlens modal, and the other has a hexagonal microlens modal.

The closed loop correction experiments were conducted with an LC WFS. The results are shown in figures 3 and 4. As shown in figure 3(a), the light point array is of size 14×14 because the area of the CCD is a little smaller than that of the whole light point array of size 16×16 due to a relay optical lens, which avoids unnecessary light reflected by the glass near

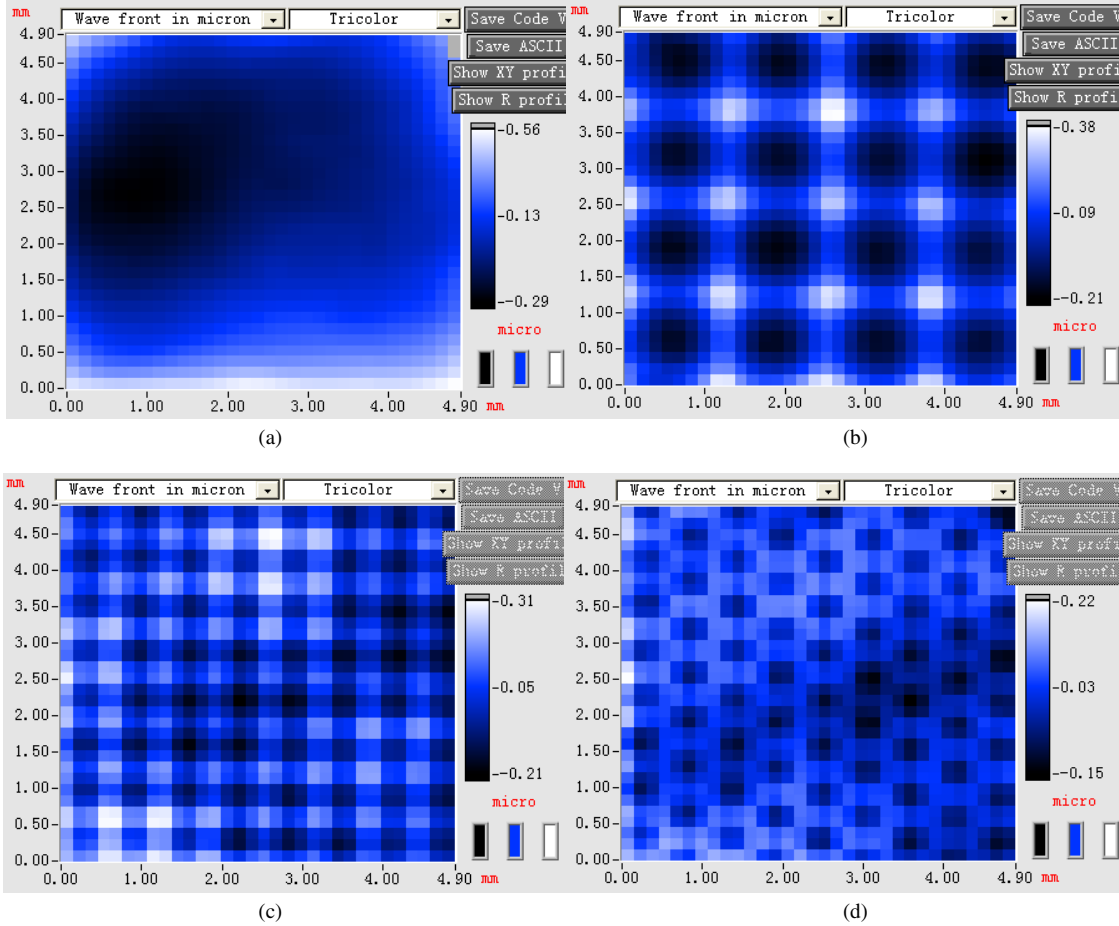


Figure 5. Measured wavefronts: (a) absolute measurement of LCOS without any gray map, (b) 4×4 LC microlens array, (c) 8×8 LC microlens array, (d) hexagonal LC microlens array corresponding to figure 1(b).

to the edge of the CCD. Red crosses denote the center position of the reference light points, and yellow crosses denote the center positions of the measured light points. The red circle as a mask shows the effective area for wavefront measurement. The wavefront is calculated with a data grid of size 32×32 . The aberrated wavefront as shown in figure 3(b) has obvious tilt and tip before correction. Then, after correction, the wavefront in figure 3(d) has no obvious tilt and tip. The residual wavefront is due to a higher order Zernike modal without correction, as shown in figure 3(c). This indicates that the coefficient values of tilt and tip Zernike modals are -0.66λ and 2.91λ before correction. After being corrected with the tilt and tip mirror, they are down to -0.01λ and 0.09λ , respectively.

In nearly the same way, we also repeated the experiment with a hexagonal LC WFS. The focus length of the LC microlens is different from that of the square modal LC WFS. Therefore, the position of the CCD in figure 2 should be adjusted and a new reference picture should be sampled. After that, the uncorrected aberration of the optical layout is different from that in figure 3. As shown in figure 4, the tilt and tip correction is also very effective when comparing the uncorrected wavefront in figure 4(b) and the corrected one in figure 4(d). As shown in figure 4(c), the coefficient values of the tilt and tip Zernike modal decreased from 0.85λ and

-3.47λ to -0.01λ and -0.07λ , respectively. It should be noted that those light points without a cross in figure 4(a) were considered as a non-effective area where no reference light points were found. On the other hand, the light points out of the mask have no bad effects on the closed loop correction because only tilt and tip terms are corrected.

In addition, the quality of the LC microlens could be evaluated by the distortion in the LC WFS optical layout. A wavefront sensor HASO 32 from Image Optics Co. was used to measure the aberration with a CCD of size $512 \text{ pixels} \times 512 \text{ pixels}$ and a microlens array of size 32×32 . As shown in figure 5(a), the absolute background aberration without any gray map on the LCOS has a PV of $0.852 \mu\text{m}$ and an rms value of $0.189 \mu\text{m}$. In this case, to check the aberration of the LC microlens array itself, we used a relative measurement mode to remove the background aberration. After removing the background aberration, the aberration of the LC microlens array is as shown in figures 5(b) to (c). As shown in figure 5(b), the measured wavefront is consistent with the theoretical wavefront for a 4×4 LC microlens array. Its PV and rms values are $0.587 \mu\text{m}$ and $0.121 \mu\text{m}$, respectively. Figure 5(c) shows the result of the LC microlens array with size 8×8 with a PV of $0.540 \mu\text{m}$ and an rms of $0.106 \mu\text{m}$. The measured LC microlens array is not as smooth as that in figure 5(b), which

is because HASO 32 has a relatively low spatial resolution of only 32×32 microlenses. For a 16×16 LC microlens array, we cannot measure its distortion with the HASO 32. Similar phenomena can also be seen in figure 5(d). Figure 5(d) shows the distortion of the LC microlens array with hexagonal arrangement as shown in figure 1(b) with a PV of $0.369 \mu\text{m}$ and an rms of $0.006 \mu\text{m}$. In fact, even for the 16×16 LC microlenses in figure 1(a), we used 32×32 LC pixels for every LC microlens, which makes the produced wavefront very consistent with the theoretical one. However, when the number of LC microlenses becomes larger, the number of LC pixels in one LC microlens will become smaller and its diffraction efficiency will decrease, which will lead to a poor light spot array on the CCD. Therefore, the number of LC microlenses produced by an LCOS will be limited by its spatial resolution. In addition to the LCOS spatial resolution problem, the aberration of the LCOS itself also needs to be considered. If we use a planar wave as reference light without compensating the distortion of the LCOS, the positions of the reference spots will be affected by the LCOS's distorted surface although by less than one wavelength. According to the reference positions obtained, the measured wavefront will not include the distortion of the LCOS itself. However, a more accurate status of the focus will be obtained after compensating the distortion of the LCOS itself.

The LC microlens for both square and hexagonal arrangements in the above experiments has no grating for an enlarged dynamic range. This is because the number of light points denoted by the yellow crosses in the circle mask will become smaller than 35, which will lead to an error when we use the first 35 Zernike modals for the wavefront reconstruction. But if the light points could be grabbed by the CCD, a large dynamic range LC WFS could also be demonstrated without any technical problems. In addition, although we only demonstrate that with our LC WFS the tilt and tip in the system could be corrected by the S-330 mirror in closed loop correction, it also could be used to control another LC wavefront corrector or deformable mirror to correct the aberrated wavefront of higher order Zernike modals.

4. Summary

In the paper, we have demonstrated a novel LC WFS based on a reflective LCOS. In addition, an optimized optical design of the WFS to save the energy of the incident light was also introduced to improve the energy utilization efficiency. As a demonstration, a closed loop wavefront correction was conducted based on the LC WFS with square and hexagonal microlens arrays, respectively. In the experiment, the corrector is a tilt and tip mirror. The Zernike coefficients of tilt and tip were decreased down to less than 0.1λ after correction in both experiments.

Acknowledgments

This work was supported by the National Natural Science Foundation of China under grant nos 60736042, 60578035 and 50473040.

References

- [1] Southwell W H 1980 Wavefront estimation from wavefront slope measurements *J. Opt. Soc. Am.* **70** 998–1006
- [2] Forest C R, Canizares C R, Neal D R, McGuirk M and Schattenburg M L 2004 Metrology of thin transparent optics using Shack–Hartmann wavefront sensing *Opt. Eng.* **43** 742–53
- [3] Lardiére O, Conan R, Bradley C, Jackson K and Herriot G 2008 A laser guide star wavefront sensor bench demonstrator for TMT *Opt. Express* **16** 5527–43 <http://www.opticsinfobase.org/abstract.cfm?URI=oe-16-8-5527>
- [4] Brooks A F, Kelly T-L, Veitch P J and Munch J 2007 Ultra-sensitive wavefront measurement using a Hartmann sensor *Opt. Express* **15** 10370–5 <http://www.opticsinfobase.org/abstract.cfm?URI=oe-15-16-10370>
- [5] Ares M, Royo S and Caum J 2007 Shack–Hartmann sensor based on a cylindrical microlens array *Opt. Lett.* **32** 769–71
- [6] Manzanera S, Canovas C, Prieto P M and Artal P 2008 A wavelength tunable wavefront sensor for the human eye *Opt. Express* **16** 7748–55 <http://www.opticsinfobase.org/abstract.cfm?URI=oe-16-11-7748>
- [7] Lane R G and Tallon M 1992 Wavefront reconstruction using a Shack–Hartmann sensor *Appl. Opt.* **31** 6902
- [8] Chernyshov A, Sterr U, Riehle F, Helmcke J and Pfund J 2005 Calibration of a Shack–Hartmann sensor for absolute measurements of wavefronts *Appl. Opt.* **44** 6419–25
- [9] Arines J, Durán V, Jaroszewicz Z, Ares J, Tajahuerce E, Prado P, Lancis J, Bará S and Climent V 2007 Measurement and compensation of optical aberrations using a single spatial light modulator *Opt. Express* **15** 15287–92 <http://www.opticsinfobase.org/abstract.cfm?URI=oe-15-23-15287>
- [10] Rha J, Voelz D G and Giles M K 2004 Reconfigurable Shack–Hartmann wavefront sensor *Opt. Eng.* **43** 251–6
- [11] Zhao L, Bai N, Li X, Ong L S, Fang Z P and Asundi A K 2006 Efficient implementation of a spatial light modulator as a diffractive optical microlens array in a digital Shack–Hartmann wavefront sensor *Appl. Opt.* **45** 90–4
- [12] Clark N and Prasad N S 1995 Dynamic wavefront sensor system using spatial light modulators *Proc. SPIE* **2566** 54–62
- [13] Wang Z, Eng S H and Alameh K 2007 Design and optimization of programmable lens array for adaptive optics *Proc. SPIE* **6414** 64140K
- [14] Ferstl M, Kuhlow B and Pawłowski E 1994 Effect of fabrication errors on multilevel Fresnel zone lenses *Opt. Eng.* **33** 1229–35
- [15] Lee Y, Gourlay J, Hossack W J, Underwood I and Walton A J 2004 Multi-phase modulation for nematic liquid crystal on silicon backplane spatial light modulators using pulse-width modulation driving scheme *Opt. Commun.* **236** 313–22
- [16] Dayton D, Sandven S, Ginglewski J, Browne S, Rogers S and McDermott S 1997 Adaptive optics using a liquid crystal phase modulator in conjunction with a Shack–Hartmann wavefront sensor and zonal control algorithm *Opt. Express* **1** 338–46 http://www.opticsinfobase.org/DirectPDFAccess/2B4C0D17-BDB9-137E-C8940EA6D24279_63213.pdf?da=1&id=63213&seq=0&CFID=18364614&CFTOKEN=33345908
- [17] Boyer C, Michau V and Rousset G 1990 Adaptive optics, interaction matrix measurements and real time control algorithms for the COME-ON project *Proc. SPIE* **1271** 63–81
- [18] Giles M K, Wendelstein N, Kohnle A and Weiss R 2004 Laboratory testing of components and systems used for advanced wavefront control *Proc. SPIE* **5553** 301–8
- [19] Rousset G 1999 *Adaptive Optics in Astronomy* ed F Roddier (Cambridge: Cambridge University Press) pp 107–14
- [20] Navarro R and Franceschini N 1998 On image quality of microlens arrays in diurnal superposition eyes *Pure Appl. Opt.* **7** L69–78